MCB
Journals.ASM.org

EMILIN1/α9β1 Integrin Interaction Is Crucial in Lymphatic Valve Formation and Maintenance

Carla Danussi,[a]* Lisa Del Bel Belluz,[a] Eliana Pivetta,[a] Teresa Maria Elisa Modica,[a] Andres Muro,[b] Bruna Wassermann,[a] Roberto Doliana,[a] Patrizia Sabatelli,[c,d] Alfonso Colombatti,[a,e,f] Paola Spessotto[a]

Experimental Oncology 2, CRO, IRCCS, National Cancer Institute, Aviano (PN), Italy[a]; International Centre for Genetic Engineering and Biotechnology, Trieste, Italy[b]; CNR-National Research Council of Italy, IGM-IOR, Bologna, Italy[c]; SC Laboratory of Muscoloskeletal Cell Biology, IOR, Bologna, Italy[d]; Department of Medical and Biomedical Sciences, University of Udine, Udine, Italy[e]; MATI (Microgravity, Ageing, Training, Immobility) Excellence Center, University of Udine, Udine, Italy[f]

Lymphatic vasculature plays a crucial role in the maintenance of tissue interstitial fluid balance. The role of functional collecting lymphatic vessels in lymph transport has been recently highlighted in pathologies leading to lymphedema, for which treatments are currently unavailable. Intraluminal valves are of paramount importance in this process. However, valve formation and maturation have not been entirely elucidated yet, in particular, the role played by the extracellular matrix (ECM). We hypothesized that EMILIN1, an ECM multidomain glycoprotein, regulates lymphatic valve formation and maintenance. Using a mouse knockout model, we show that in the absence of EMILIN1, mice exhibit defects in lymphatic valve structure and in lymph flow. By applying morphometric *in vitro* and *in vivo* functional assays, we conclude that this impaired phenotype depends on the lack of α9β1 integrin engagement, the specific lymphatic endothelial cell receptor for EMILIN1, and the ensuing derangement of cell proliferation and migration. Our data demonstrate a fundamental role for EMILIN1-integrin α9 interaction in lymphatic vasculature, especially in lymphatic valve formation and maintenance, and underline the importance of this ECM component in displaying a regulatory function in proliferation and acting as a "guiding" molecule in migration of lymphatic endothelial cells.

The lymphatic circulatory system maintains tissue fluid homeostasis. It plays a major role in the absorption of dietary fat and in the transport of lymphocytes and antigen-presenting cells to regional lymph nodes (LNs), and it provides routes for tumor cell metastasis (1). The lymphatic vasculature consists of a complex network of capillaries and collecting vessels. Lymphatic endothelial cells (LECs) in capillaries exhibit button-like junctions anchored to filaments in the extracellular matrix (ECM) that exert the necessary tension to keep the junctions open and to allow fluid entry. The collecting vessels are surrounded by a basement membrane and by smooth muscle cells (SMC)/mural cells, which are less organized than in blood vessels (2). LECs of collecting vessels have zipper-like junctions and contribute to the development of luminal valves, often present at vessel branch points, that prevent lymph backflow. These structural features allow efficient fluid uptake of protein-rich lymph from tissue interstitium by capillaries and transport of lymph back to the blood vascular system by collecting vessels (2).

In mice, valves originate around embryonic day 16 (E16) by specification of valve-forming cells. These cells express high levels of the transcription factors Prox1 and Foxc2 (3). Prox1 is required for the establishment of LEC identity (4) and Foxc2 for the onset of lymphatic valve formation (3) and positioning within the collecting vessels; its absence leads to loss of luminal valves and abnormal lymph flow (5). Following specification, valve cells delaminate from the vessel wall, extend, migrate into the lumen, and mature into heart-shaped leaflets capable of preventing lymph backflow. Downstream of Prox1 and Foxc2 and as a response to oscillatory shear stress, connexin 37 and calcineurin/NFAT regulate the formation of a ring-like valve area, valve territory delimitation, and postnatal valve maintenance (6, 7). Ultrastructural analyses demonstrate a close physical association between ECM and LECs in the valve leaflets (8, 9). Valve development is accompanied by deposition of ECM constituents, such as laminin α5 and collagen IV, and increased expression of integrin α9 (3, 10), suggesting that ECM provides structural integrity during valve morphogenesis and might control LEC functions. The α9 integrin–fibronectin (FN)-EIIIA pair has been suggested to play a determining role in the assembly of an ECM core within developing valve leaflets (10). Accordingly, the loss of α9 or FN-EIIIA affected leaflet elongation (10). However, since FN-EIIIA expression is progressively downregulated in postnatal lymphatic vasculature while α9 integrin also persists in the valves in adulthood and valves appear normal and functional in *Fn-EIIIA*-null mice at postnatal day 21 (P21) (10), we hypothesized that EMILIN1, an ECM multidomain glycoprotein (11–13) specifically expressed in lymphatic capillaries and vessels (14) and a ligand of α9 integrin (15), could represent a good candidate for the maintenance of morphologically and functionally normal valves.

EMILIN1 is implicated, among other functions, in the regulation of the growth and integrity of lymphatic capillaries (14). Accordingly, *Emilin1*$^{-/-}$ mice have an abnormal lymphatic phenotype with a significant reduction of anchoring filaments and lymphatic capillary hyperplasia, leading to a mild lymphedema associated with inefficient lymph drainage and increased leakage (14). Here, we demonstrate that EMILIN1, through its interaction

Received 8 July 2013 Returned for modification 18 August 2013
Accepted 3 September 2013
Published ahead of print 9 September 2013
Address correspondence to Paola Spessotto, pspessotto@cro.it.
* Present address: Carla Danussi, Institute for Cancer Genetics, Columbia University Medical Center, New York, New York, USA.
C.D. and L.D.B.B. contributed equally to this work.

doi:10.1128/MCB.00872-13

with α9β1 integrin on LECs, plays an essential role in the correct morphology and functional efficiency of lymphatic valves.

MATERIALS AND METHODS

Antibodies and reagents. Rat monoclonal anti-mouse EMILIN1 and mouse anti-human gC1q antibodies were produced in our laboratories as previously described (14, 16); rabbit polyclonal anti-mouse LYVE-1 and anti-Prox-1 (Abcam), mouse monoclonal anti-α9β1 integrin (clone Y9A2) and anti-α4 integrin (clone P1H4; Chemicon), goat polyclonal anti-mouse α9 integrin (R&D Systems Inc.), Cy-3-conjugated mouse antibody against α-smooth muscle actin (α-SMA) (Sigma), and rat anti-mouse PECAM-1 (CD31; BD Biosciences Europe) antibodies were used. The rabbit polyclonal anti-Ki67 proliferation marker was purchased from Abcam.

EMILIN1, secreted by 293 cells constitutively expressing the EBNA 1 protein, was obtained as previously described (17). The C-terminal domain of EMILIN1 (gC1q) and the recombinant mutant (E933A) of the integrin binding sequence of gC1q were produced as previously described (16, 18). For the production of the recombinant ED-A domain (EIIIA), the 273-bp cDNA sequence coding for the complete amino acid sequence of the mouse EIIIA domain from residue 1721 to residue 1811 of mouse fibronectin (NCBI NP_034363.1) was generated by reverse transcription (RT)-PCR using as the template mouse embryo total RNA transcribed with avian myeloblastosis virus (Promega) and amplified with Phusion *Taq* DNA polymerase (NEB) and the following specific primers: (i) 5′ CCGGATCCAACATTGATCGCCCTAAA 3′, including the underlined BamHI restriction site, and (ii) 5′ GGGGTACCTTAGGCTGTGGACTG GATTCCAATC 3′, including the underlined KpnI restriction site. The PCR product was isolated, digested with BamHI and KpnI restriction enzymes (Promega), ligated in pQE-30 expression vector with a 5′ 6×His tag (Qiagen), and then transformed in *Escherichia coli* strain M15. A clone carrying the cloned sequence was amplified, and the 6×His NH_2-tagged rEIIIA extracted from the bacterial pellet by sonication was purified using an Ni-nitrilotriacetic acid (NTA) resin column (Qiagen) according to the manufacturer's directions. The eluted recombinant fragment was then dialyzed against phosphate-buffered saline (PBS), and the concentration and purity were verified by Coomassie blue staining after SDS-PAGE on a 4 to 20% precast polyacrylamide gel (Bio-Rad Laboratories).

Mouse procedures and cell cultures. Procedures involving animals and their care were conducted according to the institutional guidelines in compliance with national laws (legislative decree no. 116/92). The Ethic Committee for Animal Experimentation (CESA) of CRO-IRCCS, Aviano (Italy), approved the study by protocols 2011/06/08/SP2 and 2012/01/25/SP1. *Emilin1*$^{-/-}$ mice (CD1 and C57BL/6 strains) and *Fn-EIIIA*$^{-/-}$ mice were generated as previously described (13, 19). Human microvascular endothelial cells–dermal lymphatic-neonatal (HMVEC-dLyNeo), human microvascular endothelial cells-lung lymphatic (HMVEC-LLy), and the media optimized for their growth were purchased from Lonza. Mouse lymphangioma endothelial cells (LAECs) were isolated following the procedure previously described (14). The cells were immortalized by means of simian virus 40 (SV40) infection (20).

Whole-mount staining. Specimens of interest were treated as previously described (14). The samples were fixed in 4% paraformaldehyde (PFA) for 18 h at 4°C. Then, the blocking solution (PBS, 0.3% Triton X-100, and 5% serum) was added for 8 h at 4°C, followed by primary-antibody incubation for 18 h at 4°C. After 5 washes with PBS–0.3% Triton X-100, the Alexa Fluor- or horseradish peroxidase (HRP)-conjugated secondary antibody was added and incubated for 18 h at 4°C. Images were acquired with a Leica TCS SP2 confocal system (Leica Microsystems) equipped with HC PL Fluotar 10×/0.30-numerical-aperture (NA), HCX PL Apo 40×/1.25- to 0.75-NA, and HCX PL Apo 63×/1.40- to 0.60-NA oil objectives, using LCS software, or captured with a Leica ICC50 camera connected to a Leica DM750 microscope equipped with an N Plan 5×/0.12-NA objective, a HI-Plan 10×/0.25-NA objective, and a 20× objective, all from Leica.

Electron microscopy. Mesenteries were dissected from P21 mice, fixed with 2.5% glutaraldehyde in 0.1 M sodium cacodylate buffer (pH 7.4) for 3 h, washed in 0.1 M sodium cacodylate buffer overnight, and fixed with 1% osmium tetroxide in 0.1 M sodium cacodylate buffer as previously described (13). All samples were dehydrated with ethanol and embedded in Epon E812. Serial semithin cross sections of collecting lymphatic vessels were stained with toluidine blue. Ultrathin sections were obtained from several blocks, stained with lead citrate and uranyl acetate, and observed in a Philips EM 400 transmission electron microscope (TEM) operated at 100 kV.

Cell adhesion assay. The quantitative centrifugal assay for fluorescence-based cell adhesion (CAFCA) was performed as previously described (21). CAFCA miniplates were coated with ECM substrates. Cells were labeled with the vital fluorochrome calcein AM (Molecular Probes) for 15 min at 37°C and then aliquoted into the bottom CAFCA miniplates, which were centrifuged to synchronize the contact of the cells with the substrate. The miniplates were then incubated for 20 min at 37°C and then mounted together with a similar CAFCA miniplate to create communicating chambers for subsequent reverse centrifugation. The relative numbers of cells bound to the substrate and cells that fail to bind to the substrate were estimated by top/bottom fluorescence detection in a computer-interfaced GeniusPlus microplate reader (Tecan).

Migration assays. (i) Wound-healing assay. Cells were allowed to grow to confluence in 12-well tissue culture plates, and a 200-μl tip was used to introduce a scratch in the monolayer. The wells were imaged and recorded at ×10 magnification with a Leica AF6000 fluorescence microscope system (Leica Microsystem) for 20 h postscratch at 15-min intervals.

(ii) Transwell chamber migration/haptotaxis assay. Cellular migration was assessed by fluorescence-assisted transmigration invasion and motility assay (FATIMA) as previously described, with slight modification (21). We measured the capability of cells to move in the presence of a guidance cue, i.e., as a consequence of a haptotactic response to components of the ECM. For this reason, the undersides of the inserted membranes were coated with 10 μg/ml gC1q or EIIIA recombinant fragments to create a gradient for the ECM molecules. Cells were fluorescently tagged with Fast DiI (Molecular Probes) and added to the upper sides of the inserts. After 8 h, the membranes were cut off and mounted for analysis under a fluorescence microscope (Leica TCS SP2). The cells on the underside of the filter (transmigrated cells) were counted.

EMILIN1 silencing. For production of lentiviral vectors, 293FT cells were transfected with pLP1, pLP2, pVSVG, and scrambled pLKO or pLKO short hairpin RNA (shRNA) EMILIN1 no. 33 lentiviral transfer vectors (Mission shRNA bacterial glycerol stock; Sigma-Aldrich). The lentiviral vector yield was determined by measuring the amount of p24 Gag protein using an HIV-1 p24 Antigen ELISA Kit (PerkinElmer) according to the manufacturer's instructions. Wild-type (WT) LAECs (2.8×10^4) were seeded in 6-well dishes 1 day before transduction. The cells were exposed for 24 h to lentivirus vector preparations with multiplicities of infection (MOIs) ranging from 5 to 15 and supplemented with Polybrene. Transduced cells were grown in selective medium containing puromycin for 5 days.

Lymphangiography. Two microliters of 5-mg/ml fluorescein isothiocyanate (FITC)-dextran (mass, ~2,000 kDa; Invitrogen) was injected into the tails of anesthetized mice (P21 or 6 weeks old). After different time intervals, mice were sacrificed, and the draining lymph nodes and collectors were imaged using a Leica M205 FA stereomicroscope and a Leica DFC310 FX digital camera (Leica Microsystems).

Computer-assisted morphometric analyses. To quantitatively evaluate valve density, samples were analyzed using a Leica TCS SP2 confocal system detecting simultaneous positivity for Prox1 and α-SMA. The series obtained were then processed with Volocity 3D image analysis software (PerkinElmer). On the optical acquired images, computer-assisted morphometric analyses were performed using imageJ software (http://rsb.info.nih.gov).

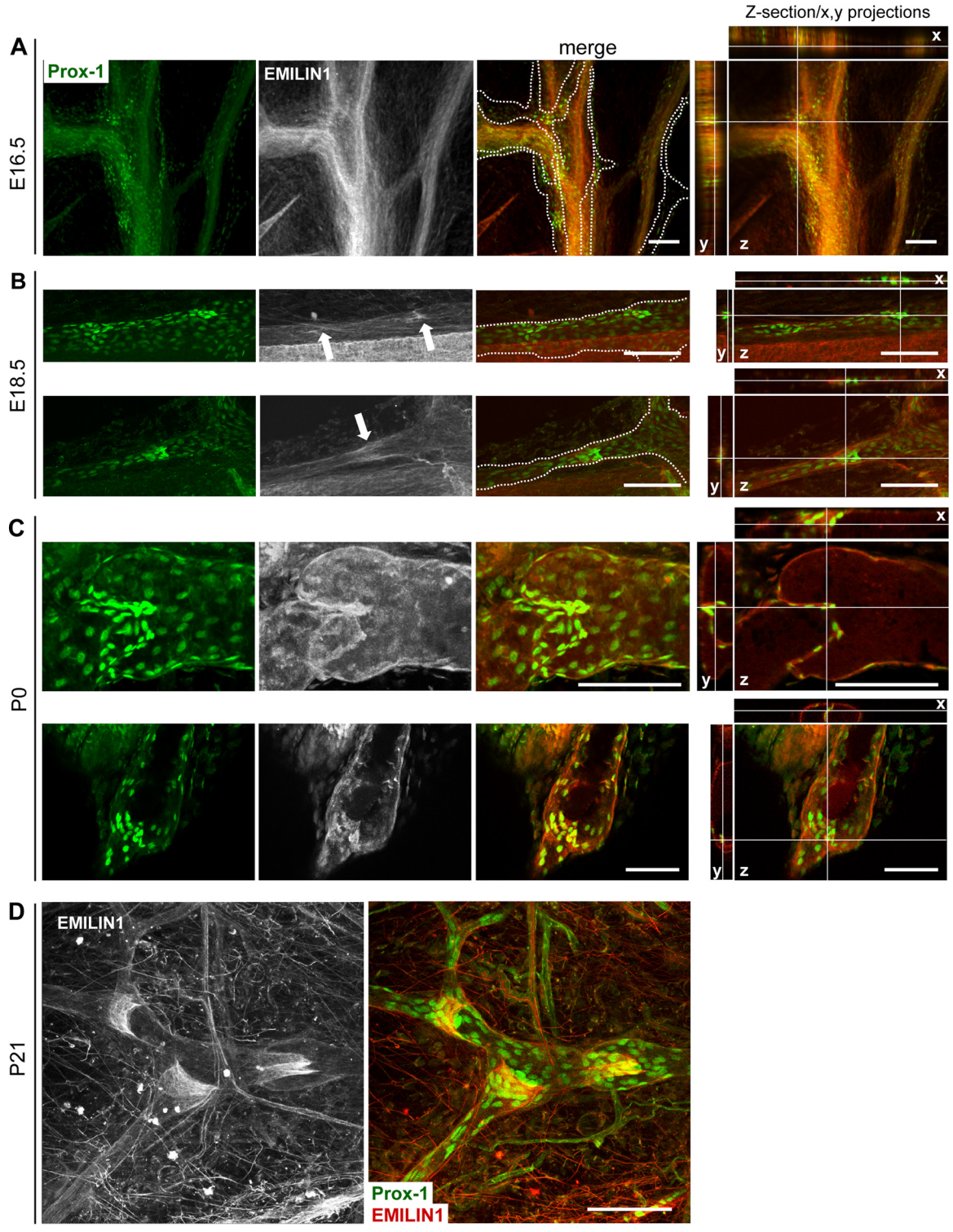

FIG 1 Expression of EMILIN1 in developing and mature lymphatic valves. Shown is immunofluorescence staining of mesenteric lymphatic vessels (A, B, and C) and adult ear skin (D) with antibodies against Prox1 (green) and EMILIN1 (pseudocolored gray or red). Representative images from tissues taken from embryos at the indicated ages (A and B) and from the postnatal period (P0 [C] and P21 [D]) are shown. The arrows in panel B indicate more evident staining for EMILIN1 associated with endothelial cells expressing high levels of Prox1. The dotted line outlines the lymphatic vessels. Z-sections of mesenteric lymphatic vessels and the corresponding *x* and *y* projections showing a clear association between EMILIN1 and Prox-1 staining are provided for panels A, B, and C. Scale bars, 100 μm.

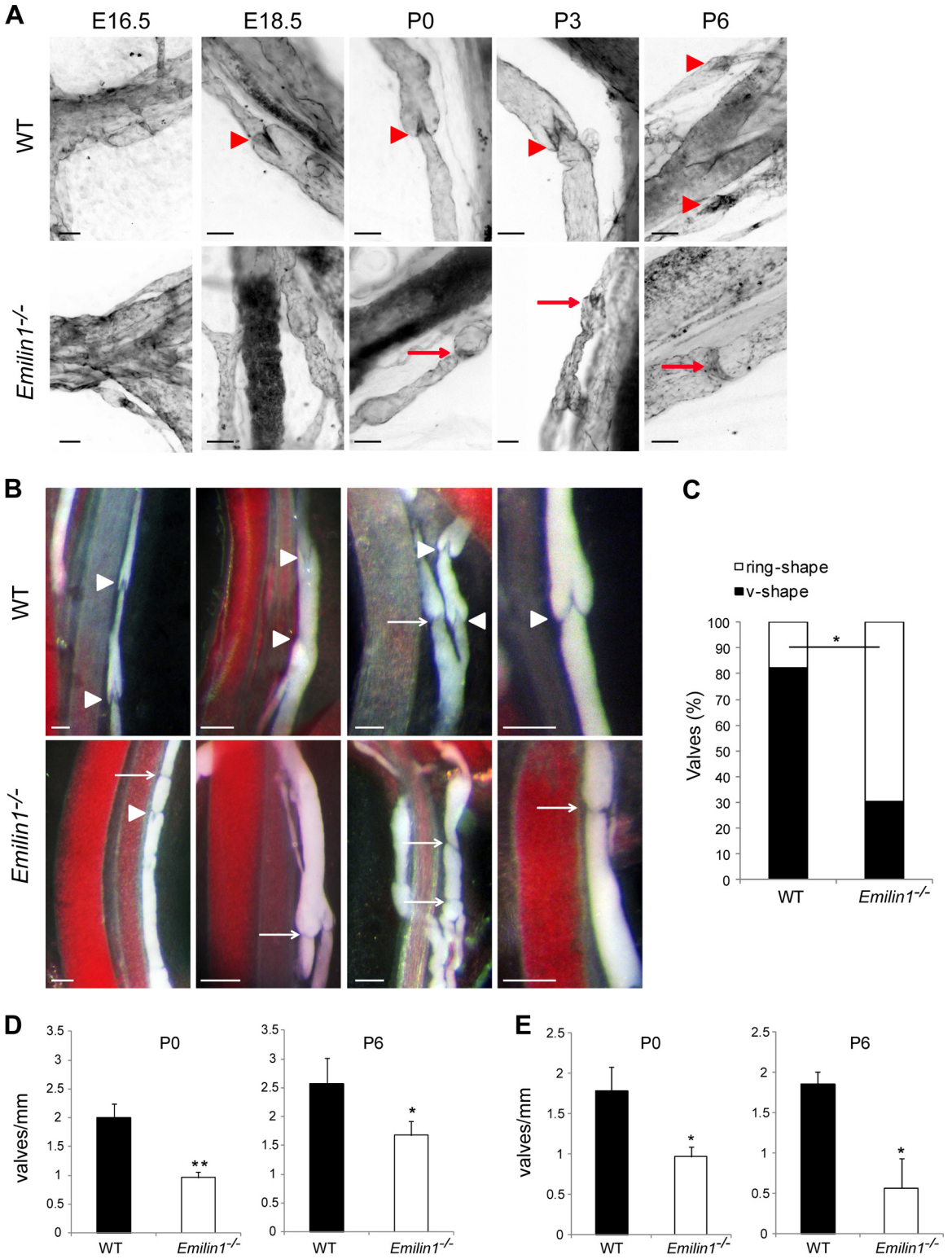

FIG 2 Abnormal lymphatic valves in *Emilin1*$^{-/-}$ mice. (A) PECAM-1 immunohistochemistry of mesenteric vessels and luminal valves of embryonic (E16.5 and E18.5) and postnatal (P0, P3, and P6) WT and *Emilin1*$^{-/-}$ mice. Note the difference in shape of WT (arrowheads) and *Emilin1*$^{-/-}$ (arrows) valves. (B) Luminal valves in chyle-filled mesenteric P6 WT and *Emilin1*$^{-/-}$ mice. The arrows and arrowheads indicate abnormal (ring-shaped) and normal (V-shaped) valves, respectively. (C) Morphological evaluation of valve shape in P6 WT and *Emilin1*$^{-/-}$ mesenteric lymphatic vessels. Black bar, normal V-shaped valves; white bar, abnormal ring-shaped valves ($n = 3$ animals per genotype; more than 100 valves were counted for each genotype). *, $P < 0.05$ (χ^2 test). (D and E) Quantification of the luminal valves in neonatal and postnatal WT and *Emilin1*$^{-/-}$ mesenteric lymphatic vessels of CD1 (P0 and P6) (D) and C57BL/6 (P0 and P6) (E) mice (means and standard deviations [SD]; $n = 3$ animals per genotype with 10 vessels each; *, $P < 0.05$; **, $P < 0.01$; unpaired Student's *t* test). Scale bars, 50 μm (A) and 100 μm (B).

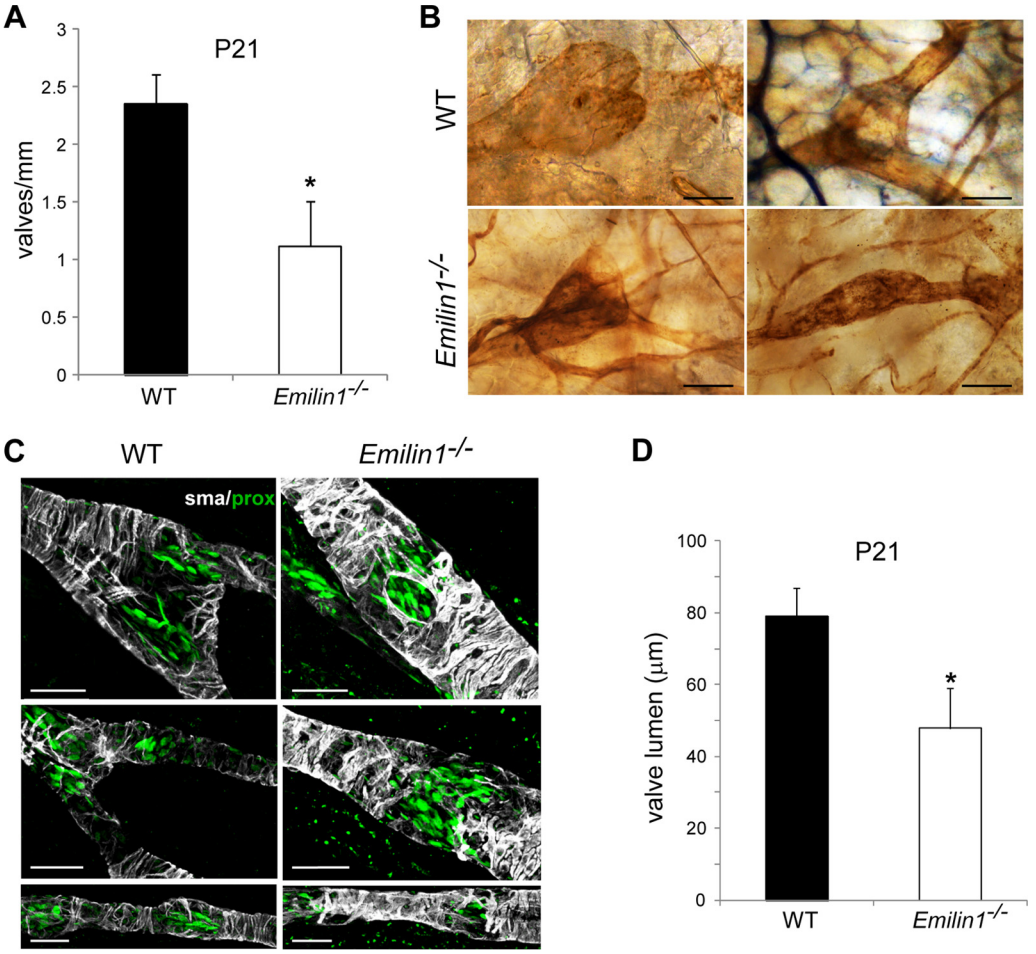

FIG 3 Defects of lymphatic collectors in adult animals. (A) Quantification of the luminal valves in adult (P21) CD1 WT and *Emilin1*$^{-/-}$ mesenteric lymphatic vessels (means and SD; $n = 3$ animals per genotype with 10 vessels each; *, $P = 0.01$). (B) PECAM-1 staining of ear vessels in 6-month-old C57BL/6 mice. Note the well-formed V-shaped valves in WT animals compared to the narrow structures of collecting vessels in *Emilin1*$^{-/-}$ mice. (C) Adult lymphatic mesenteric vessels (P21) stained for α-SMA (gray) and Prox1 (green) of WT and *Emilin1*$^{-/-}$ mice. (D) Lumen sizes of the valves in adult (P21) WT and *Emilin1*$^{-/-}$ mesenteric lymphatic vessels. Z-stack images were collected from whole-mount samples stained for α-SMA and Prox1; the resulting three-dimensional (3D) reconstruction by Volocity software combined with *x* and *y* projections was used to highlight and calculate the smallest (d_s) and largest (d_l) diameters of the valve lumen. The values obtained from calculation $[(d_s + d_l)/2]$ are reported in the graph. Four mice per genotype (at least 5 valves/mesentery) were examined. *, $P < 0.01$. Scale bars, 25 μm (C) and 50 μm (B).

Statistical analysis. The statistical significance of the results was determined by using the two-tailed unpaired Student *t* test to determine whether two data sets were significantly different. To compare more than two data sets, we additionally performed a one-way analysis of variance, followed by Tukey's *post hoc* test. A χ^2 test was used in some analyses, as indicated. A *P* value of <0.05 was considered significant.

RESULTS

EMILIN1 is expressed in developing and mature lymphatic valves. EMILIN1 expression along all lymphatic vessels and the structural capillary defects associated with inefficient lymph drainage and mild lymphedema observed in *Emilin1*$^{-/-}$ mice (14) prompted us to examine if EMILIN1 might be involved in the formation, maturation, and function of collecting-vessel luminal valves. During mouse development, the formation of collecting vessels occurs in late embryonic and early postnatal life (3, 22). At E16.5, mesenteric lymphatic vessels formed a Prox1-positive vascular network with defined clusters of Prox1-positive cells indicative of valve formation (Fig. 1A). At this stage, EMILIN1 expression in lymphatic endothelia was very low, while it was already high in blood vessels (Fig. 1A). At E18.5, the lymphatic vessels formed constrictions with more evident staining for EMILIN1 (Fig. 1B, arrows). This expression data suggested that EMILIN1 upregulation in lymphatics correlated with the initiation of valve leaflet development. The staining of lymphatic vessels with EMILIN1 antibodies in neonatal (P0) and young adult mice strongly highlighted this ECM constituent near the cells of the luminal valves (Fig. 1C and D). A very close physical association between EMILIN1 and LECs in the valve leaflets was clearly evident already at P0 (Fig. 1C); later (P21), the entire valve matrix core was positive for EMILIN1 with the staining concentrated on the free edges of the leaflet fibers (Fig. 1D).

***Emilin1*$^{-/-}$ mice display abnormal and functionally deficient lymphatic valves.** Staining for PECAM-1, which is strongly expressed in LECs forming the valve leaflets, demonstrated that most of the valves in neonatal *Emilin1*$^{-/-}$ mice appeared as horizontal ring-shaped constrictions (Fig. 2A, arrows) rather than V-shaped structures, as in WT mice (arrowheads). In *Emilin1*$^{-/-}$

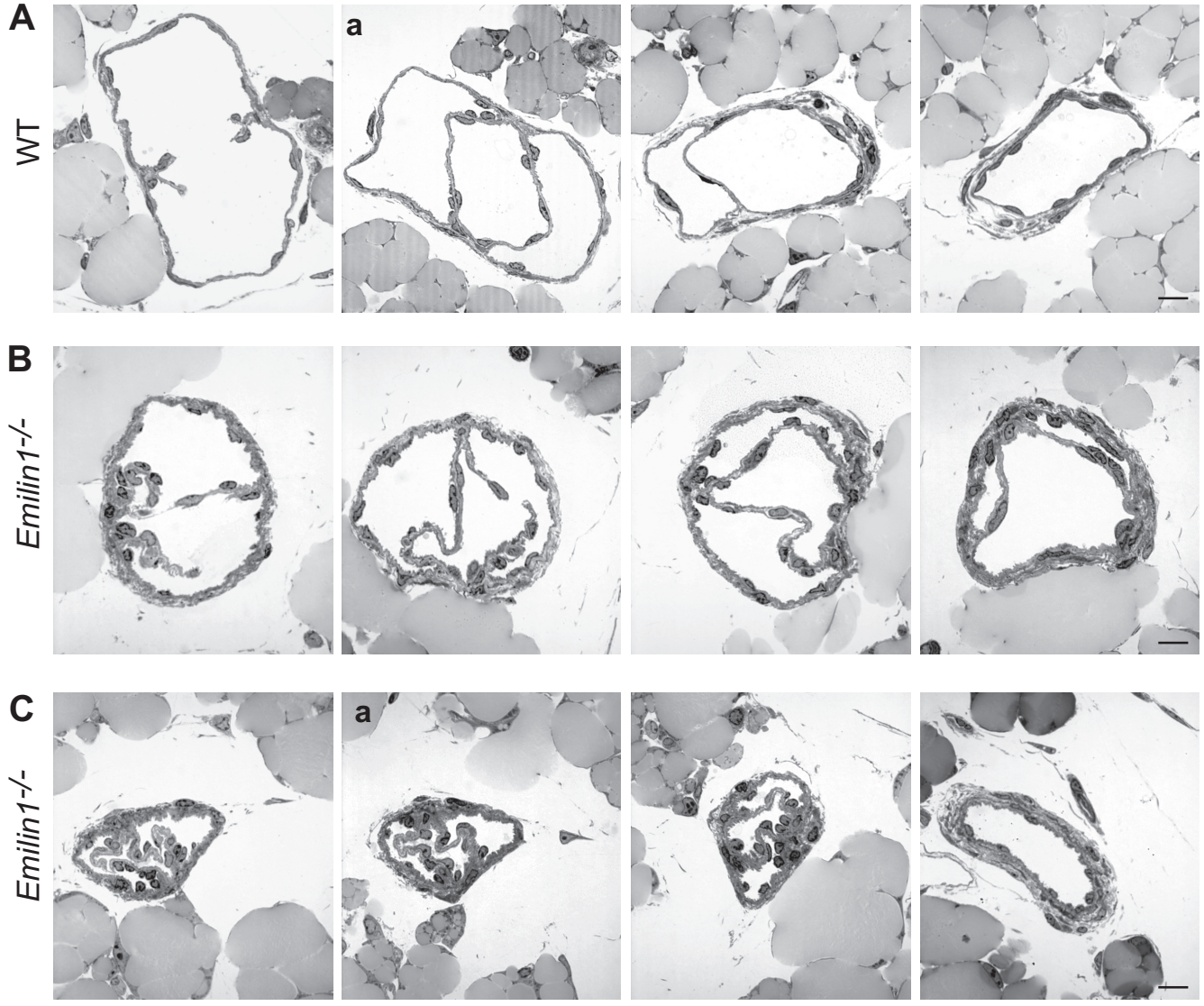

FIG 4 Abnormal lymphatic collectors and valves in *Emilin1*$^{-/-}$ adult mice. Shown are serial semithin cross sections of P21 WT (A) and two representative *Emilin1*$^{-/-}$ (B and C) mesenteric valves. Note the increased thickness of the lymphatic wall in *Emilin1*$^{-/-}$ mice. The lumen of collecting vessels in the right-hand panel appears contracted, with folded valve leaflets. The sections marked "a" in panels A and C were subjected to ultrastructural analysis as shown in Fig. 5. Scale bars, 25 μm.

E18.5 embryos, only immature structures were detected, while in WT mice, well-formed valves were already observed (Fig. 2A). In addition, *Emilin1*$^{-/-}$ collectors sometimes appeared rather throttled and more convoluted and twisted than in WT mice (Fig. 2A and B). The different valve morphology was even more evident in chyle-filled mesenteric collecting vessels (Fig. 2B). In P6 *Emilin1*$^{-/-}$ mice, the percentage of V-shaped structures was significantly lower than in WT mice, suggesting that the deposition of EMILIN1 was necessary for well-defined valve leaflet formation and setting (Fig. 2C). *Emilin1*$^{-/-}$ mice also had fewer luminal valves: an analysis performed on mesenteric collecting vessels, after staining for both Prox1 and α-SMA, demonstrated that the distance between valves was significantly greater in *Emilin1*$^{-/-}$ mice than in their WT littermates (Fig. 2D). The abnormal pattern observed in CD1 mice was confirmed in inbred newborn *Emilin1*$^{-/-}$ C57BL/6 mice (Fig. 2E) and, more importantly, in adult animals in both mesenteric and cutaneous vessels (Fig. 3A and B). At P21, the collecting vessels in *Emilin1*$^{-/-}$ mice were intensely stained for α-SMA, indicating a more pronounced coverage of mural cells (Fig. 3C). The lumen corresponding to the valve region was smaller in *Emilin1*$^{-/-}$ mice than in WT mice (Fig. 3D). The analysis of semithin sections confirmed that the vessel walls of *Emilin1*$^{-/-}$ mice were thicker and that the valve lumen appeared contracted with folded valve leaflets compared to WT mice, suggesting that there were more LECs in the leaflets of *Emilin1*$^{-/-}$ mice (Fig. 4). In addition, ultrathin sections confirmed that these subendothelial cells had an SMC/myofibroblast-like phenotype characterized by the presence of caveolae, cytoplasmic filaments, and a proper basement membrane in *Emilin1*$^{-/-}$ collecting vessels (Fig. 5).

Very likely, the morphological valve defects of *Emilin1*$^{-/-}$ mice could reduce the functionality of fluid transport. To evaluate

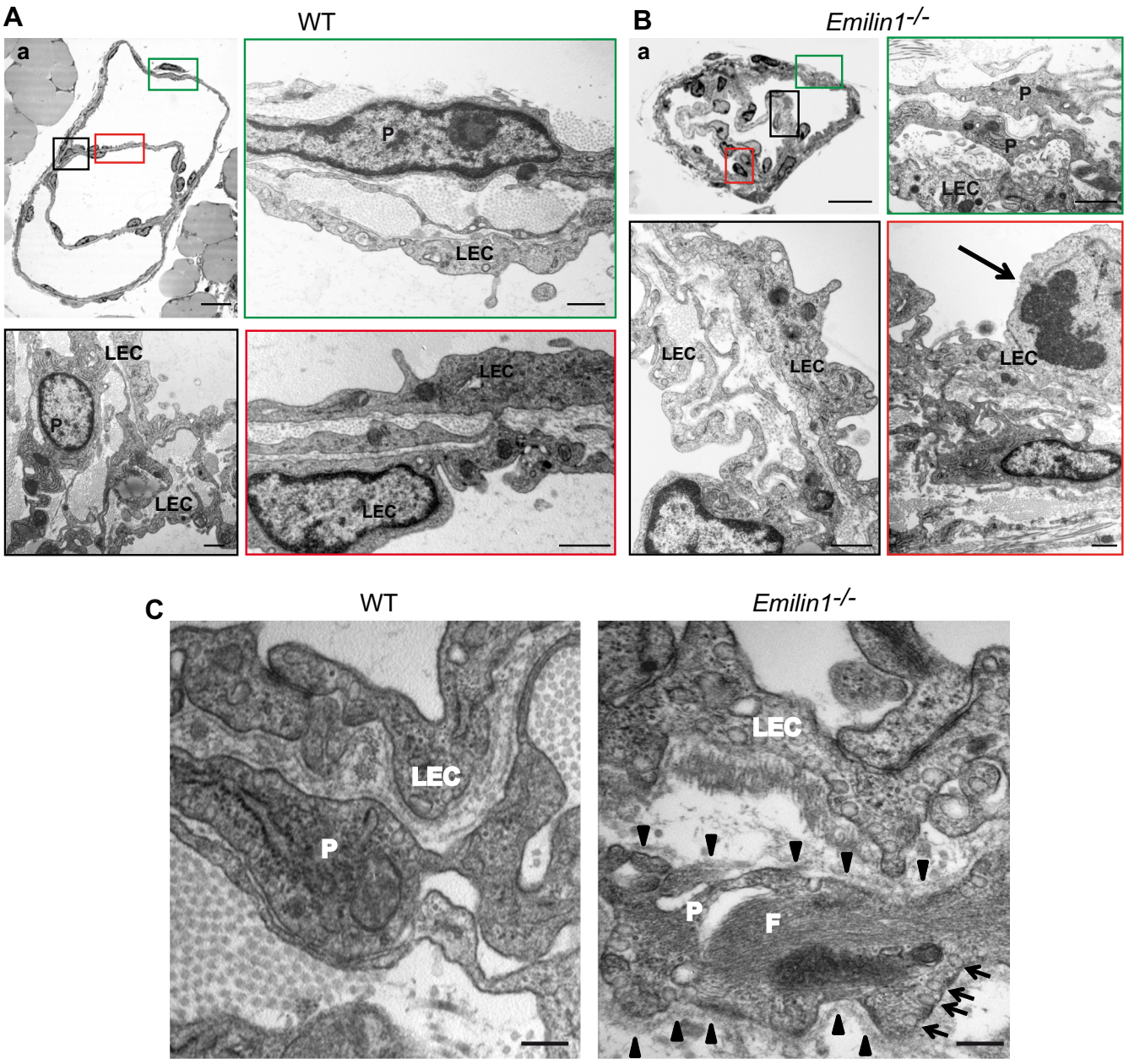

FIG 5 Ultrastructural analysis of mesenteric valves and lymphatic wall in adult mice. (A and B) TEM analysis of P21 WT (A) and *Emilin1*$^{-/-}$ (B) mesenteric valves. The colored boxes in the semithin sections (upper left panels, corresponding to sections Aa and Ca, respectively, from Fig. 4) represent the areas that were selected for ultrathin sections. *Emilin1*$^{-/-}$ mice show an increased number of mural cells/pericytes (P), which display a SMC/myofibroblast-like phenotype, and folded LECs. The arrow in panel B indicates a mitotic LEC. (C) TEM analysis of P21 WT and *Emilin1*$^{-/-}$ mesenteric lymphatic vessel walls showing increased numbers of caveolae (arrows) and cytoplasmic filaments (F) and the presence of a basement membrane (arrowheads) at the surface of one representative *Emilin1*$^{-/-}$ mural cell/pericyte. Scale bars, 25 μm (Aa and Ba), 1 μm (A and B), and 500 nm (C).

if valve function was compromised, we investigated uptake and transport to draining LNs of subcutaneously injected high-molecular-weight fluorescent dextran in P21 mice. The FITC-dextran injected into the tail was rapidly (5 min) drained via the collectors into the iliac LNs, and after 30 min, mesenteric LNs also became visible (Fig. 6A and inset) in WT mice. In contrast, the fluorescent dye labeled LNs more faintly and slowly, and collectors were difficult to visualize in *Emilin1*$^{-/-}$ mice (Fig. 6A). A similar difference in staining of draining LNs was evident in 6-week-old mice, indicating that valve anomalies contributed to the persistence of reduced lymphatic functionality in weanling, as well as in adult, *Emilin1*$^{-/-}$ mice (Fig. 6B). Kinetic analysis of FITC-dextran lymph node uptake confirmed slower dye transport in P21 *Emilin1*$^{-/-}$ mice than in their WT littermates (Fig. 6C).

EMILIN1 colocalizes with α9 integrin in the valve leaflets. The ECM has important functions in providing structural integrity during lymphatic-valve morphogenesis (8–10). Specifically, the α9 integrin–FN-EIIIA interaction is involved in the formation of the valve leaflet ECM core during vessel development (10). However, FN-EIIIA expression is progressively downregulated af-

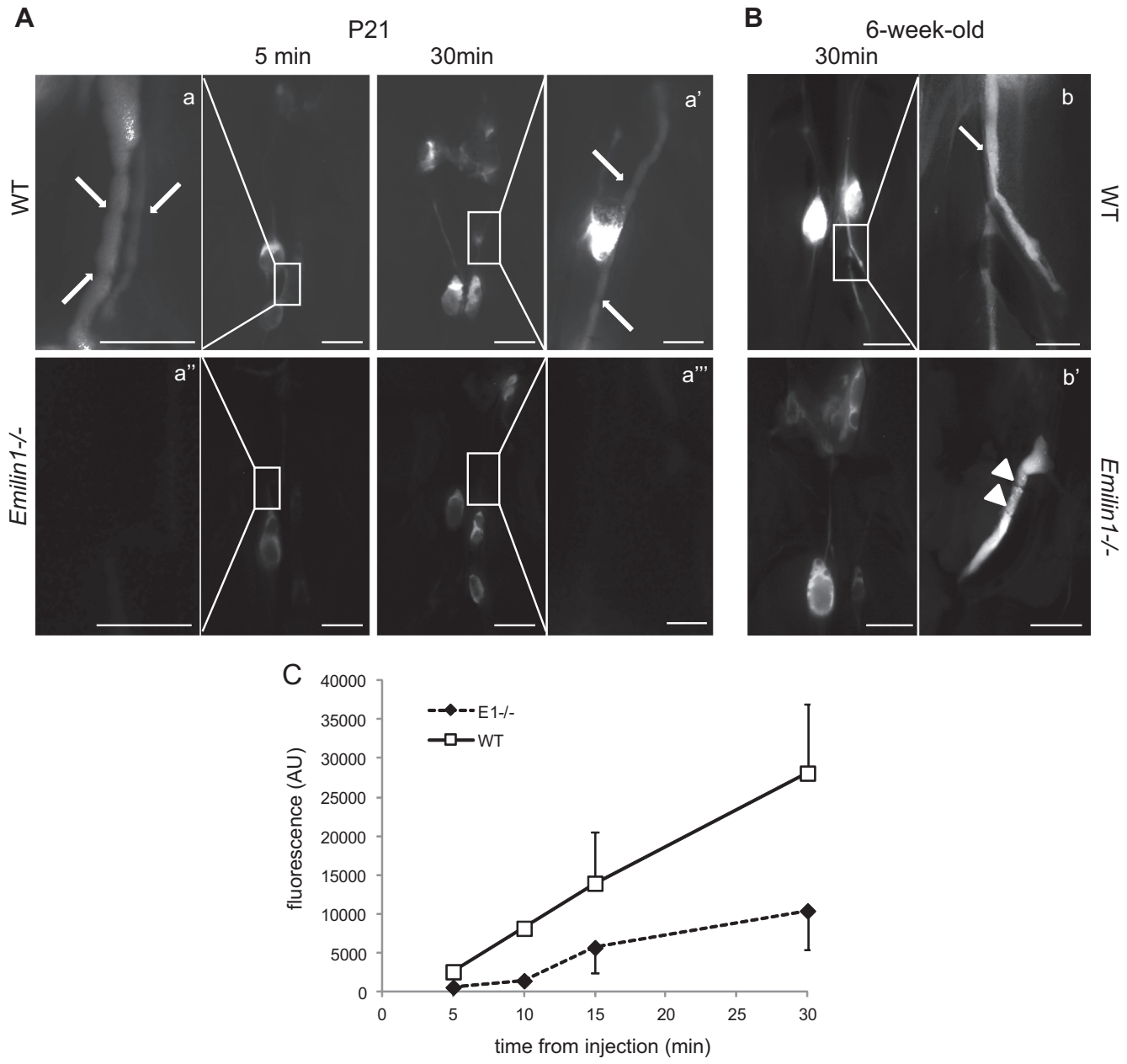

FIG 6 EMILIN1 deficiency leads to impaired lymphatic collector function. FITC-dextran (2,000 kDa) was subcutaneously injected into the tails of WT and *Emilin1*$^{-/-}$ mice at P21 (A) and at 6 weeks (B) to visualize the draining lymphatic vasculature and lymph nodes. The mice were sacrificed after injection at the indicated times. Low-magnification images were taken to visualize lymph nodes, and high-magnification images (a, a′, a″, a‴, b, and b′) were taken to detail collectors corresponding to the boxed areas. Note the difference in fluorescence intensity between WT and *Emilin1*$^{-/-}$ draining lymph nodes and collectors. The arrows and arrowheads indicate V- and ring-shaped valves, respectively. (C) Draining lymph nodes (inguinal, iliac, and mesenteric) were removed 30 min after injection and measured with a computer-interfaced GeniusPlus microplate reader (Tecan, Italy). Arbitrary fluorescence units (AU) in the graph represent the sums obtained from the fluorescence values of all draining lymph nodes/mouse. The graph reports the means ± SD of three independent experiments ($n = 4$ animals per genotype). Scale bar, 2 mm (0.5 mm in a, a′, a″, a‴, b, and b′).

ter birth, while α9 integrin remains present in the adult valves (10). It remained to be determined if any candidate ECM molecule other than FN-EIIIA could play the role of cognate ligand for this integrin. We investigated the expression and localization of EMILIN1 and α9 integrin in embryonic, neonatal, and mature mesenteric lymphatic vessels. EMILIN1 was detected in both blood and lymphatic vessel structures from E18.5 (Fig. 1A and 7A). At this stage, a clear association with α9 integrin was detected (Fig. 7A). EMILIN1 was present as a thin network in the mesenteric membrane at P0, but its fibers were thicker in the lymphatic valves (Fig. 7B, arrows, and C), which were highly positive for α9 integrin. Confocal longitudinal cross sections of mesenteric valves revealed EMILIN1 deposition on both luminal and abluminal sides of the valve LECs already at P0 (Fig. 7C and D). Colocalization with α9 integrin in the valve leaflets was well highlighted at P6 (Fig. 7E).

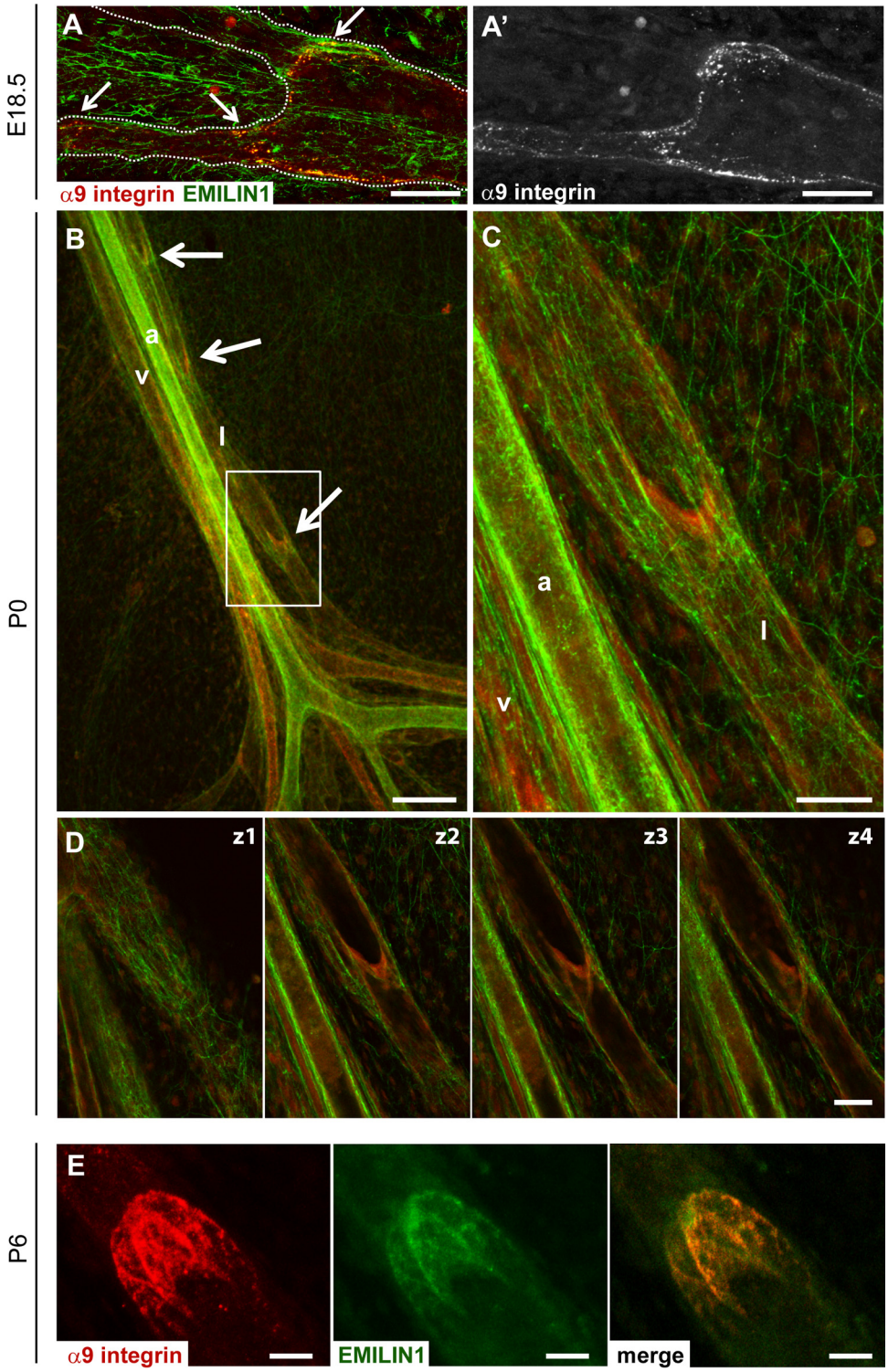

FIG 7 EMILIN1 colocalizes with α9 integrin in valve leaflets. Immunofluorescence staining for the localization of EMILIN1 (green) and α9 integrin (A′, red or gray) in embryonic (E18.5) (A and A′), neonatal (P0) (B, C, and D), and mature (P6) (E) mesenteric lymphatic vessels. The arrows indicate lymphatic valves, which were positive for both EMILIN1 and α9 integrin staining. (C) Magnification of the boxed area in panel B. The dotted lines in panel A outline the lymphatic vessels. (B and C) Mesenteric vessels are indicated as follow: a, artery; v, vein; l, lymphatic. (D) Four confocal longitudinal cross sections of a mesenteric valve showing EMILIN1 expression at both abluminal (z1) and luminal (z2, z3, and z4) sides of the valve and colocalization with α9 integrin in the valve leaflets. (E) Representative P6 mesenteric lymphatic valve stained for EMILIN1 (green) and α9 integrin (red). Scale bars, 150 μm (B), 50 μm (A, C, and D), and 25 μm (E).

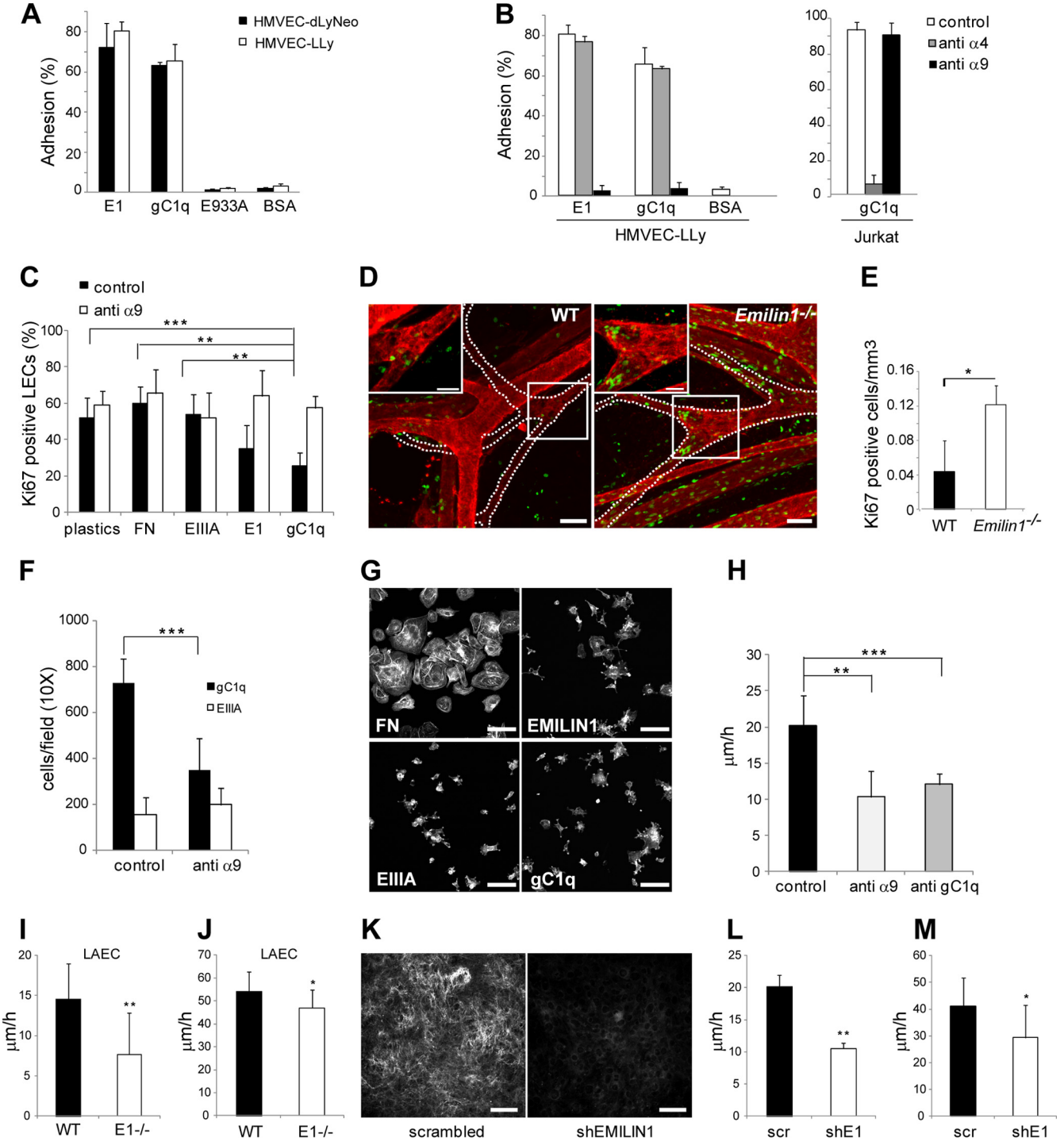

FIG 8 EMILIN1 is an α9 integrin-specific ligand in the lymphatic vasculature system. (A) Percentages of HMVEC-LLy and HMVEC-dLyNeo cells adhering to EMILIN1 (E1), gC1q, E933A, and bovine serum albumin (BSA). The data are expressed as means and SD of three independent experiments with 6 replicates. (B) Adhesion of HMVEC-LLy and Jurkat cells (positive control for α4 integrin expression). The cells were preincubated with anti-α4 integrin subunit monoclonal antibody (MAb) (P1H4) or anti-α9 integrin subunit MAb (Y9A2). The data are expressed as means and SD of three independent experiments with 6 replicates. (C) Proliferation of HMVEC-LLy cells cultured on tissue culture plates (plastics) and incubated for 48 h in the presence of fibronectin, EIIIA, E1, or gC1q. The data are expressed as mean percentages and SD of the number of Ki67-positive cells of three independent experiments. Six fields were examined for each condition. (D) Representative images of Ki67 (green) and α-SMA (red) staining of WT and *Emilin1*$^{-/-}$ P6 mesenteric vessels. The dotted lines outline the lymphatic vessels. The insets are magnifications of the boxed areas showing the presence of a higher number of Ki67-positive cells in *Emilin1*$^{-/-}$ lymphatic valves. (E) Quantification of the Ki67-positive cells of luminal valve-associated areas in WT and *Emilin1*$^{-/-}$ P6 mesenteric lymphatic vessels. Z-stack images were collected from whole-mount samples; the resulting 3D reconstruction by Volocity software was used to highlight and calculate the valve area and count the associated Ki67-positive cells. Four mice per genotype (at least 10 valves/mesentery) were examined. (F) Haptotactic movement of HMVEC-dLyNeo cells toward

EMILIN1-α9 interaction regulates LEC proliferation and migration. HMVEC-LLy and HMVEC-dLyNeo, both expressing α9 integrin (data not shown), were allowed to adhere to EMILIN1 or its functional adhesion gC1q domain or to a recombinant nonfunctional mutant (E933A) (18). Both lung and dermal LECs strongly adhered to EMILIN1 and gC1q (Fig. 8A). Although both HMVEC-LLy and HMVEC-dLyNeo express α4 integrin (data not shown), which is highly homologous to α9 (23, 24) and a known receptor of EMILIN1 or gC1q (15, 16), they exhibited no α4-dependent adhesion to EMILIN1 (Fig. 8B), likely because the α4β1 receptor was inactive (25). On the contrary, the complete inhibition of LEC attachment to both EMILIN1 and gC1q with the function-blocking anti-α9β1 integrin antibody further demonstrated that this was the integrin used by LECs to interact with EMILIN1. To investigate the possible mechanisms by which EMILIN1-α9 interaction regulates lymphatic valve formation and maturation, we examined LEC proliferative capacity *in vitro*. The engagement of EMILIN1 or of its functional domain, gC1q, significantly reduced LEC proliferation (Fig. 8C). The addition of function-blocking α9 integrin antibody fully rescued this inhibition, confirming the specificity of this effect by the EMILIN1-gC1q–α9 cognate pair (Fig. 8C). On the other hand, neither FN nor recombinant EIIIA fragment altered LEC numbers (Fig. 8C). The increased LEC proliferation in the absence of EMILIN1-α9 interaction, as shown by *in vitro* assays and the hyperplastic appearance of *Emilin1*$^{-/-}$ valves seen in TEM images (Fig. 4), suggested a possible mechanism for the formation of defective valves in *Emilin1*$^{-/-}$ mice. This hypothesis was supported by the increased proliferation detected in *Emilin1*$^{-/-}$ P6 mice: the number of Ki67-positive cells in lymphatic valves was about 4-fold higher than in WT counterparts (Fig. 8D and E). EMILIN1-α9 interaction also influenced cell migration: haptotaxis experiments with human HMVEC-dLyNeo highlighted that EMILIN1, through its gC1q domain, engages α9 integrin, favoring LEC migration (Fig. 8F). This interaction is specific, since EIIIA did not trigger any LEC movement (Fig. 8F). This was not due to a defective binding ability: the numbers of LECs adhering on FN and EMILIN1, as well as on EIIIA and gC1q, fragments were very similar. Pronounced cellular spreading was detected only for FN, since cells likely employed α5 integrin to adhere to this substrate with the consequent formation of well-defined adhesion plaques not visible when α4 or α9 integrins are used (16) (Fig. 8G). The involvement of EMILIN1-α9 engagement in LEC migration was confirmed in a wound-healing scratch assay performed on HMVEC-dLyNeo in the presence of function-blocking antibodies against α9 integrin or against gC1q (Fig. 8H). The results indicated that LEC movement was partially induced by gC1q and was α9β1 dependent. We then performed scratch assays on WT and *Emilin1*$^{-/-}$ LAECs and found that cells expressing EMILIN1 more rapidly moved to close the wounds, and the difference was even more evident when LAECs migrated in the absence of growth factors and supplements normally present in the complete medium for LECs (Fig. 8I and J). EMILIN1 likely guided the movement of LAECs, as the same reduction in velocity was obtained when EMILIN1 expression was abrogated (Fig. 8K to M).

EMILIN1 contributes to valve formation, maintenance, and function more than FN-EIIIA. To clarify the relative contributions of FN-EIIIA and EMILIN1, we followed a genetic approach. *Fn-EIIIA*-null mice were crossed with *Emilin1*-null mice to obtain double-knockout (KO) mice, and the luminal mesenteric valves of a large number of collecting vessels in P0 and P6 animals were counted and their morphology was examined (Fig. 9). The numbers of valves in *Fn-EIIIA*$^{-/-}$ and WT mice were similar, whereas in *Emilin1*$^{-/-}$ mice, there were 58% fewer valves at P0 and 64% fewer at P6. Double-KO mice displayed a reduction at both ages indistinguishable from that of *Emilin1*$^{-/-}$ mice. Abnormal/immature valves were nearly doubled only in *Emilin1*$^{-/-}$ and double-KO mice compared to *Fn-EIIIA*$^{-/-}$ and WT mice at P0. At P6, *Fn-EIIIA*$^{-/-}$ mice displayed 43% ring valves versus 25% in WT mice ($P = 0.05$); at this age, *Emilin1*$^{-/-}$ and double-KO mice had about 55% ring valves ($P < 0.01$) (Fig. 9A to E).

The less significant role of FN-EIIIA in valve morphogenesis and function compared to EMILIN1 was further confirmed by semithin and ultrathin TEM analysis and *in vivo* lymphangiography (Fig. 9F and data not shown): the valves of P21 *Fn-EIIIA*$^{-/-}$ mice had a normal morphology, and the SMC/mural cells did not show any evidence of caveolae or cytoplasmic filaments or a proper basement membrane, as detected in *Emilin1*$^{-/-}$ mice (Fig. 5). Accordingly, dye transport was equivalent to that in WT mice at P21 (data not shown). Altogether, these data suggested that the defects detected in newborn (P0 and P6) *Fn-EIIIA*$^{-/-}$ mice do not affect proper valve structure and function in adulthood.

DISCUSSION

In a previous study, we confined our morphofunctional analysis in *Emilin1*$^{-/-}$ mice to the lymphatic capillaries and demonstrated that EMILIN1 deficiency resulted in a significant reduction of anchoring filaments of capillaries with structural and functional defects and increased leakage (14). In the current study, we identified EMILIN1 and its cognate α9β1 integrin as a critical receptor-ECM pair playing a fundamental role in collector luminal valve formation and maintenance. The finding of a decreased total number of valves and of a high percentage of valves arrested at the ring shape stage in *Emilin1*$^{-/-}$ mice provided a more thorough explanation for the reduced functionality of the lymphatic circulatory system and the ensuing mild lymphedema (14). Moreover, the unusual myofibroblast-like/mural cell coverage, particularly of the valve areas, detected in *Emilin1*$^{-/-}$ mice suggests a novel role of EMILIN1 and casts new light on the valve maturation process.

gC1q or EIIIA in the presence or absence of the function-blocking monoclonal anti-α9 integrin subunit. (G) Phalloidin staining for actin cytoskeleton visualization of HMVEC-dLyNeo after 1 h of adhesion on FN, EMILIN1, EIIIA, or gC1q. (H) Wound-healing scratch performed on HMVEC-dLyNeo in the presence of the function-blocking monoclonal anti-α9 integrin subunit or of the monoclonal antibody anti-gC1q. Scratch healing was determined by measuring the shortest distance between scratch edges at 0 and 20 h in each field of view. At least 3 different fields were measured per scratch. (I and J) Wound-healing assays of WT and *Emilin1*$^{-/-}$ (E1-/-) LAECs. The graphs report the speed of closure (μm/h) of WT and *Emilin1*$^{-/-}$ LAECs in the presence of culture medium without (I) or enriched with (J) supplements and growth factors. (K) Immunodetection for EMILIN1 staining of LAEC transduced with scrambled or short hairpin RNA EMILIN1 (shEMILIN1) lentiviral particles. (L and M) Velocity of scrambled (scr) and EMILIN1 silenced (shE1) LAECs in a scratch assay in the presence of culture medium without (L) or enriched with (M) supplements and growth factors. The data shown in the graphs are the means and SD of three independent experiments each. *, $P < 0.05$; **, $P \leq 0.02$; ***, $P = 0.0001$. Scale bars, 50 μm (D, G, and K) and 25 μm (insets).

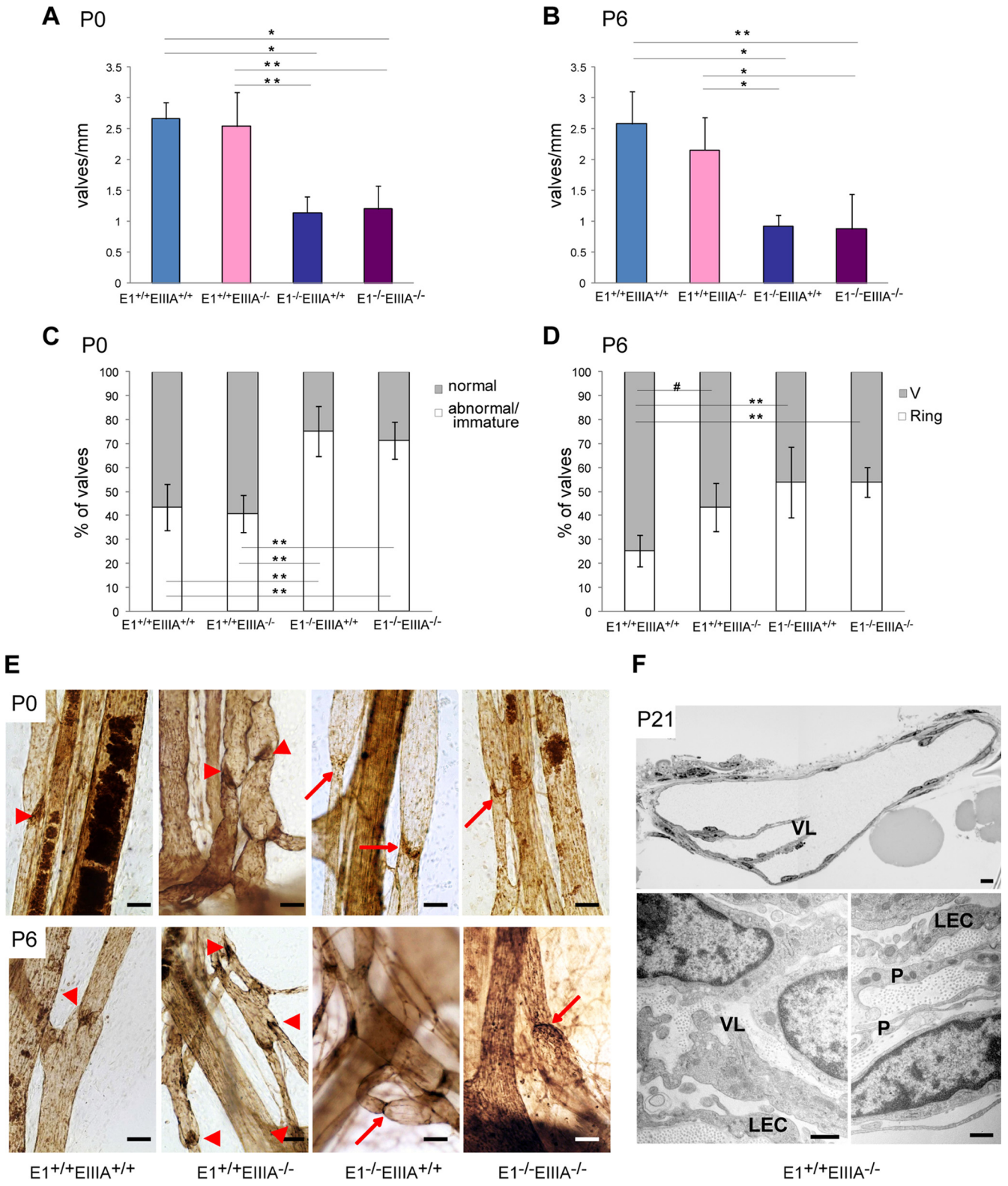

FIG 9 EMILIN1 and FN-EIIIA contributions to valve formation and maturation. *Fn-EIIIA*-null mice were crossed with *Emilin1*-null mice. The luminal valve numbers (A and B) and morphological analyses (C and D) of mesenteric lymphatic vessels in neonatal (P0) (A and C) and postnatal (P6) (B and D) mice of the resulting genotypes are reported in the graphs. (E) Mesenteric vessels stained for PECAM-1 of P0 and P6 WT ($E1^{+/+}$ $EIIIA^{+/+}$), $E1^{+/+}$ $EIIIA^{-/-}$, $E1^{-/-}$ $EIIIA^{+/+}$, and double-KO ($E1^{-/-}$ $EIIIA^{-/-}$) mice. The arrowheads and arrows indicate normal V-shaped and abnormal ring-shaped valves, respectively. (F) Morphological analyses of semithin (top) and ultrathin (bottom) cross sections of mesenteric collecting vessels of $E1^{+/+}$ $EIIIA^{-/-}$ mice at P21 showing normal features of the valve leaflets (VL), endothelial cells (LEC), and mural cells/pericytes (P). The data shown in panels A and B are the means and SD ($n = 3$ to 6 animals per genotype with more than 10 vessels each). The data in panels C and D were obtained from 3 to 6 animals per genotype (more than 100 valves each). #, $P = 0.05$; *, $P < 0.05$; **, $P < 0.01$ (a one-way analysis of variance followed by Tukey's *post hoc* test was performed). Scale bars, 50 μm (E), 20 μm (F, top), and 1 μm (F, bottom).

Many findings relate α9β1 integrin to the development/function of the lymphatic vascular system (10, 26–29). α9β1-null mice, which die around P12 of massive chylothorax, have specific defects in lymphatic valves that appear as horizontal constrictions rather than V shaped, whereas the lymphatic vasculature apparently undergoes normal development (26). α9β1 interacts with a relatively large number of ECM ligands, including tenascin C, osteopontin, VCAM-1, and FN-EIIIA (10, 24, 30–33). Null mutations in some of these α9β1 ligands did not affect the development of a normal lymphatic phenotype (34–37). In contrast, the fibronectin FN-EIIIA variant is the main α9 integrin ligand during luminal valve morphogenesis, and α9 integrin-EIIIA regulates fibronectin fibrillogenesis by LECs *in vitro* (10). However, as already pointed out by the authors, the altered valve phenotype of P6 *Fn-EIIIA*-null mice normalized at P21, suggesting lower penetrance or the existence of a compensatory mechanism in P21 *Fn-EIIIA*$^{-/-}$ mice with the involvement of other α9 integrin ligands. The present finding that *Emilin1*$^{-/-}$ mice had a valve morphology as severe as double-KO *Fn-EIIIA*$^{-/-}$ *Emilin1*$^{-/-}$ mice and that fluid transport had no alterations in adult *Fn-EIIIA*$^{-/-}$ mice while it was impaired in *Emilin1*$^{-/-}$ mice indicated that EMILIN1 also plays a major role in valve maintenance. The crucial impact of EMILIN1 on valve morphogenesis was further confirmed by ultrastructural analysis: the increased thickness of the collecting-vessel wall of P21 *Emilin1*$^{-/-}$ mice was accompanied in the valve area by folded leaflets, whereas the valves of P21 *Fn-EIIIA*$^{-/-}$ mice had a normal V-shaped morphology.

α9β1 integrin was first demonstrated to be an EMILIN1 receptor in skin (15). The increased proliferation of HMVEC *in vitro* and the increased number of proliferating Ki67-positive LECs in valves suggested a deregulated proliferation program of LECs, as reported for basal keratinocytes of *Emilin1*$^{-/-}$ mice (15). Also, *in vitro*, LEC adhesion to and migration on EMILIN1 was specifically regulated by α9 integrin. One could speculate that *in vivo* the EMILIN1-α9 interaction regulates the proper and specific migration of LECs to settle in the lymphatic vessel areas where valves originate. Altogether, these results suggest that EMILIN1 and its cognate receptor α9β1 play a dual role in valve morphogenesis: not only in contributing to the structural integrity of the valve core but also in "guiding" the migration of LECs and their controlled proliferation to form functional valve leaflets. Since the region where lymphatic valves arise has to be tightly controlled, this additional regulatory role of EMILIN1 in the differentiation and growth program of cells forming valve leaflets could be hypothesized.

Immature collecting vessels lack myofibroblast-like/mural cells, and only at later stages do they acquire sparse coverage, but the valve areas are usually devoid of these cells (3). Among the various molecules involved in the establishment and maintenance of lymphatic collectors, Sema3A is the only one known to date that plays a role in regulating coverage by SMC/mural cells (38): accordingly, Sema3a-null mice exhibit abnormal SMC coating. α-SMA staining showed that EMILIN1 absence determined extended SMC coating in the valve-forming areas that are usually devoid of SMC in WT mice. α-SMA staining in *Emilin1*$^{-/-}$ mice showed similar extended SMC coverage in the valve areas. These cells also acquired a myofibroblast-like/mural morphology with unique changes, including caveolae, cytoplasmic filaments, and a proper basement membrane.

Emilin1$^{-/-}$ mice display a compound defect of the lymphatic vasculature that involves the capillaries and the collecting-vessel valves. The severe morphological alterations of endoluminal valves likely contribute to the impaired fluid transport, resulting in the mild lymphedema detected only in adults and absent in *Emilin1*$^{-/-}$ mouse embryos (C. Danussi, A. Colombatti, and P. Spessotto, unpublished data). This finding is in striking contrast to the fatal bilateral chylothorax of α9 integrin-deficient mice (26), which apparently show only severe endoluminal valve defects with shorter leaflets and fewer LECs (10).

The absence of chylothorax in *Emilin1*$^{-/-}$ mice suggests that the defects in α9β1-null mice cannot fully be explained by the mere lack of EMILIN1-α9β1 integrin interaction. It is conceivable that myofibroblast-like/mural cells positioned on collecting vessels are part of the flow-regulating mechanism and should cooperate with the valves to prevent lymph backflow during contraction. We speculate that the compensatory element that overcomes the absence of EMILIN1-α9β1 integrin engagement and culminates in a less severe deficit in lymph propulsion is represented by the enhanced LEC cellularity in the valve leaflets and by the unusual myofibroblast-like/mural cell coverage, particularly of the valve areas.

While investigations on perivascular myofibroblast-like/mural cell recruitment and function in fluid flow were beyond the scope of the present study, the EMILIN1 model could be exploited in the future to investigate the role, if any, of the increased coverage by myofibroblast-like/mural cells in order to explain human lymphedema severity. This also takes into account the fact that transforming growth factor β1 (TGF-β1) is a strong inducer of fibroblast-myofibroblast terminal differentiation (39); thus, since EMILIN1 inhibits TGF-β1 maturation (40), the increased TGF-β1 levels detected in *Emilin1*$^{-/-}$ mice (15, 40) might contribute to an increase of myofibroblast-like/mural cell transdifferentiation.

In conclusion, we conceive the multifaceted function of EMILIN1 in lymphatic vessels as (i) participating in the structural integrity of capillaries (14) and valve leaflets, (ii) contributing to the homeostatic control of proliferation, and (iii) playing a regulatory role as a "guiding" ECM molecule for migration of LECs.

ACKNOWLEDGMENTS

This work was supported by AIRC (IG 10119) and Ministry of Health (RF-2010-2309719) grants to P.S.

We thank G. M. Bressan for providing *Emilin1*$^{-/-}$ mice, M. Schiappacassi for help in production of lentiviral vectors, Stefania Moica for her contribution to whole-mount staining, and Jerry Polesel for help with statistical analyses.

REFERENCES

1. **Cueni LN, Detmar M.** 2008. The lymphatic system in health and disease. Lymphat. Res. Biol. **6:**109–122.
2. **Tammela T, Alitalo K.** 2010. Lymphangiogenesis: molecular mechanisms and future promise. Cell **140:**460–476.
3. **Norrmen C, Ivanov KI, Cheng J, Zangger N, Delorenzi M, Jaquet M, Miura N, Puolakkainen P, Horsley V, Hu J, Augustin HG, Yla-Herttuala S, Alitalo K, Petrova TV.** 2009. FOXC2 controls formation and maturation of lymphatic collecting vessels through cooperation with NFATc1. J. Cell Biol. **185:**439–457.
4. **Wigle JT, Oliver G.** 1999. Prox1 function is required for the development of the murine lymphatic system. Cell **98:**769–778.
5. **Petrova TV, Karpanen T, Norrmen C, Mellor R, Tamakoshi T, Finegold D, Ferrell R, Kerjaschki D, Mortimer P, Yla-Herttuala S, Miura N, Alitalo K.** 2004. Defective valves and abnormal mural cell recruitment

underlie lymphatic vascular failure in lymphedema distichiasis. Nat. Med. **10:**974–981.
6. **Kanady JD, Dellinger MT, Munger SJ, Witte MH, Simon AM.** 2011. Connexin37 and Connexin43 deficiencies in mice disrupt lymphatic valve development and result in lymphatic disorders including lymphedema and chylothorax. Dev. Biol. **354:**253–266.
7. **Sabine A, Agalarov Y, Maby-El HH, Jaquet M, Hagerling R, Pollmann C, Bebber D, Pfenniger A, Miura N, Dormond O, Calmes JM, Adams RH, Makinen T, Kiefer F, Kwak BR, Petrova TV.** 2012. Mechanotransduction, PROX1, and FOXC2 cooperate to control connexin37 and calcineurin during lymphatic-valve formation. Dev. Cell **22:**430–445.
8. **Lauweryns JM, Boussauw L.** 1973. The ultrastructure of lymphatic valves in the adult rabbit lung. Z. Zellforsch.Mikrosk.Anat. **143:**149–168.
9. **Navas V, O'Morchoe PJ, O'Morchoe CC.** 1991. Lymphatic valves of the rat pancreas. Lymphology **24:**146–154.
10. **Bazigou E, Xie S, Chen C, Weston A, Miura N, Sorokin L, Adams R, Muro AF, Sheppard D, Makinen T.** 2009. Integrin-alpha9 is required for fibronectin matrix assembly during lymphatic valve morphogenesis. Dev. Cell **17:**175–186.
11. **Colombatti A, Bressan GM, Castellani I, Volpin D.** 1985. Glycoprotein 115, a glycoprotein isolated from chick blood vessels, is widely distributed in connective tissue. J. Cell Biol. **100:**18–26.
12. **Bressan GM, Daga-Gordini D, Colombatti A, Castellani I, Marigo V, Volpin D.** 1993. Emilin, a component of elastic fibers preferentially located at the elastin-microfibrils interface. J. Cell Biol. **121:**201–212.
13. **Zanetti M, Braghetta P, Sabatelli P, Mura I, Doliana R, Colombatti A, Volpin D, Bonaldo P, Bressan GM.** 2004. EMILIN-1 deficiency induces elastogenesis and vascular cell defects. Mol. Cell. Biol. **24:**638–650.
14. **Danussi C, Spessotto P, Petrucco A, Wassermann B, Sabatelli P, Montesi M, Doliana R, Bressan GM, Colombatti A.** 2008. Emilin1 deficiency causes structural and functional defects of lymphatic vasculature. Mol. Cell. Biol. **28:**4026–4039.
15. **Danussi C, Petrucco A, Wassermann B, Pivetta E, Modica TM, Belluz LB, Colombatti A, Spessotto P.** 2011. EMILIN1-{alpha}4/{alpha}9 integrin interaction inhibits dermal fibroblast and keratinocyte proliferation. J. Cell Biol. **195:**131–145.
16. **Spessotto P, Cervi M, Mucignat MT, Mungiguerra G, Sartoretto I, Doliana R, Colombatti A.** 2003. Beta 1 Integrin-dependent cell adhesion to EMILIN-1 is mediated by the gC1q domain. J. Biol. Chem. **278:**6160–6167.
17. **Spessotto P, Bulla R, Danussi C, Radillo O, Cervi M, Monami G, Bossi F, Tedesco F, Doliana R, Colombatti A.** 2006. EMILIN1 represents a major stromal element determining human trophoblast invasion of the uterine wall. J. Cell Sci. **119:**4574–4584.
18. **Verdone G, Doliana R, Corazza A, Colebrooke SA, Spessotto P, Bot S, Bucciotti F, Capuano A, Silvestri A, Viglino P, Campbell ID, Colombatti A, Esposito G.** 2008. The solution structure of EMILIN1 globular C1q domain reveals a disordered insertion necessary for interaction with the alpha4beta1 integrin. J. Biol. Chem. **283:**18947–18956.
19. **Muro AF, Chauhan AK, Gajovic S, Iaconcig A, Porro F, Stanta G, Baralle FE.** 2003. Regulated splicing of the fibronectin EDA exon is essential for proper skin wound healing and normal lifespan. J. Cell Biol. **162:**149–160.
20. **Danussi C, Petrucco A, Wassermann B, Modica TM, Pivetta E, Belluz LD, Colombatti A, Spessotto P.** 2012. An EMILIN1-negative microenvironment promotes tumor cell proliferation and lymph node invasion. Cancer Prev. Res. **5:**1131–1143.
21. **Spessotto P, Lacrima K, Nicolosi PA, Pivetta E, Scapolan M, Perris R.** 2009. Fluorescence-based assays for in vitro analysis of cell adhesion and migration. Methods Mol. Biol. **522:**221–250.
22. **Makinen T, Adams RH, Bailey J, Lu Q, Ziemiecki A, Alitalo K, Klein R, Wilkinson GA.** 2005. PDZ interaction site in ephrinB2 is required for the remodeling of lymphatic vasculature. Genes Dev. **19:**397–410.
23. **Palmer EL, Ruegg C, Ferrando R, Pytela R, Sheppard D.** 1993. Sequence and tissue distribution of the integrin alpha 9 subunit, a novel partner of beta 1 that is widely distributed in epithelia and muscle. J. Cell Biol. **123:**1289–1297.
24. **Taooka Y, Chen J, Yednock T, Sheppard D.** 1999. The integrin alpha9beta1 mediates adhesion to activated endothelial cells and transendothelial neutrophil migration through interaction with vascular cell adhesion molecule-1. J. Cell Biol. **145:**413–420.
25. **Calzada MJ, Zhou L, Sipes JM, Zhang J, Krutzsch HC, Iruela-Arispe ML, Annis DS, Mosher DF, Roberts DD.** 2004. Alpha4beta1 integrin mediates selective endothelial cell responses to thrombospondins 1 and 2 in vitro and modulates angiogenesis in vivo. Circ. Res. **94:**462–470.
26. **Huang XZ, Wu JF, Ferrando R, Lee JH, Wang YL, Farese RV, Jr, Sheppard D.** 2000. Fatal bilateral chylothorax in mice lacking the integrin alpha9beta1. Mol. Cell. Biol. **20:**5208–5215.
27. **Vlahakis NE, Young BA, Atakilit A, Sheppard D.** 2005. The lymphangiogenic vascular endothelial growth factors VEGF-C and -D are ligands for the integrin alpha9beta1. J. Biol. Chem. **280:**4544–4552.
28. **Kajiya K, Hirakawa S, Ma B, Drinnenberg I, Detmar M.** 2005. Hepatocyte growth factor promotes lymphatic vessel formation and function. EMBO J. **24:**2885–2895.
29. **Mishima K, Watabe T, Saito A, Yoshimatsu Y, Imaizumi N, Masui S, Hirashima M, Morisada T, Oike Y, Araie M, Niwa H, Kubo H, Suda T, Miyazono K.** 2007. Prox1 induces lymphatic endothelial differentiation via integrin alpha9 and other signaling cascades. Mol. Biol. Cell **18:**1421–1429.
30. **Yokosaki Y, Palmer EL, Prieto AL, Crossin KL, Bourdon MA, Pytela R, Sheppard D.** 1994. The integrin alpha 9 beta 1 mediates cell attachment to a non-RGD site in the third fibronectin type III repeat of tenascin. J. Biol.Chem. **269:**26691–26696.
31. **Yokosaki Y, Matsuura N, Sasaki T, Murakami I, Schneider H, Higashiyama S, Saitoh Y, Yamakido M, Taooka Y, Sheppard D.** 1999. The integrin alpha(9)beta(1) binds to a novel recognition sequence (SVVYGLR) in the thrombin-cleaved amino-terminal fragment of osteopontin. J. Biol. Chem. **274:**36328–36334.
32. **Eto K, Puzon-McLaughlin W, Sheppard D, Sehara-Fujisawa A, Zhang XP, Takada Y.** 2000. RGD-independent binding of integrin alpha9beta1 to the ADAM-12 and -15 disintegrin domains mediates cell-cell interaction. J. Biol. Chem. **275:**34922–34930.
33. **Majumdar M, Tarui T, Shi B, Akakura N, Ruf W, Takada Y.** 2004. Plasmin-induced migration requires signaling through protease-activated receptor 1 and integrin alpha(9)beta(1). J. Biol. Chem. **279:**37528–37534.
34. **Gurtner GC, Davis V, Li H, McCoy MJ, Sharpe A, Cybulsky MI.** 1995. Targeted disruption of the murine VCAM1 gene: essential role of VCAM-1 in chorioallantoic fusion and placentation. Genes Dev. **9:**1–14.
35. **Forsberg E, Hirsch E, Frohlich L, Meyer M, Ekblom P, Aszodi A, Werner S, Fassler R.** 1996. Skin wounds and severed nerves heal normally in mice lacking tenascin-C. Proc. Natl. Acad. Sci. U. S. A. **93:**6594–6599.
36. **Fukamauchi F, Mataga N, Wang YJ, Sato S, Youshiki A, Kusakabe M.** 1996. Abnormal behavior and neurotransmissions of tenascin gene knockout mouse. Biochem. Biophys. Res. Commun. **221:**151–156.
37. **Liaw L, Birk DE, Ballas CB, Whitsitt JS, Davidson JM, Hogan BL.** 1998. Altered wound healing in mice lacking a functional osteopontin gene (spp1). J. Clin. Invest. **101:**1468–1478.
38. **Jurisic G, Maby-El HH, Karaman S, Ochsenbein AM, Alitalo A, Siddiqui SS, Ochoa PC, Petrova TV, Detmar M.** 2012. An unexpected role of semaphorin3A-neuropilin-1 signaling in lymphatic vessel maturation and valve formation. Circ. Res. **111:**426–436.
39. **Evans RA, Tian YC, Steadman R, Phillips AO.** 2003. TGF-beta1-mediated fibroblast-myofibroblast terminal differentiation—the role of Smad proteins. Exp. Cell Res. **282:**90–100.
40. **Zacchigna L, Vecchione C, Notte A, Cordenonsi M, Dupont S, Maretto S, Cifelli G, Ferrari A, Maffei A, Fabbro C, Braghetta P, Marino G, Selvetella G, Aretini A, Colonnese C, Bettarini U, Russo G, Soligo S, Adorno M, Bonaldo P, Volpin D, Piccolo S, Lembo G, Bressan GM.** 2006. Emilin1 links TGF-beta maturation to blood pressure homeostasis. Cell **124:**929–942.